the FEBS Journal

Diversity and junction residues as hotspots of binding energy in an antibody neutralizing the dengue virus

Hugues Bedouelle[1], Laurent Belkadi[1], Patrick England[1,*], J. Iñaki Guijarro[2], Olesia Lisova[1], Agathe Urvoas[1], Muriel Delepierre[2] and Philippe Thullier[3]

1 Unit of Molecular Prevention and Therapy of Human Diseases (CNRS-FRE 2849), Institut Pasteur, Paris, France
2 Unité de RMN des Biomolécules (CNRS-URA 2185), Institut Pasteur, Paris, France
3 Département de Biologie des Agents Transmissibles, Centre de Recherche du Service de Santé des Armées, La Tronche, France

Keywords
antibody; complementary determining region; dengue virus; gene rearrangement; molecular recognition

Correspondence
H. Bedouelle, Unit of Molecular Prevention and Therapy of Human Diseases (CNRS-FRE 2849), Institut Pasteur, 28 rue Docteur Roux, 75724 Paris Cedex 15, France
Fax: +33 1 40 61 35 33
Tel.: +33 1 45 68 83 79
E-mail: hbedouel@pasteur.fr

***Present address**
Plate-forme de Biophysique des Macromolécules et de leurs Interactions, Institut Pasteur, Paris, France

(Received 17 August 2005, revised 6 October 2005, accepted 31 October 2005)

doi:10.1111/j.1742-4658.2005.05045.x

Dengue is a re-emerging viral disease, affecting approx. 100 million individuals annually. The monoclonal antibody mAb4E11 neutralizes the four serotypes of the dengue virus, but not other flaviviruses. Its epitope is included within the highly immunogenic domain 3 of the envelope glycoprotein E. To understand the favorable properties of recognition between mAb4E11 and the virus, we recreated the genetic events that led to mAb4E11 during an immune response and performed an alanine scanning mutagenesis of its third hypervariable loops (H-CDR3 and L-CDR3). The affinities between 16 mutant Fab fragments and the viral antigen (serotype 1) were measured by a competition ELISA in solution and their kinetics of interaction by surface plasmon resonance. The diversity and junction residues of mAb4E11 (D segment; V_H-D, D-J_H and V_L-J_L junctions) constituted major hotspots of interaction energy. Two residues from the D segment (H-Trp96 and H-Glu97) provided > 85% of the free energy of interaction and were highly accessible to the solvent in a three-dimensional model of mAb4E11. Changes of residues (L-Arg90 and L-Pro95) that statistically do not participate in the contacts between antibodies and antigens but determine the structure of L-CDR3, decreased the affinity between mAb4E11 and its antigen. Changes of L-Pro95 and other neutral residues strongly decreased the rate of association, possibly by perturbing the topology of the electrostatic field of the antibody. These data will help to improve the properties of mAb4E11 for therapeutic applications and map its epitope precisely.

Dengue is a disease which is re-emerging, viral and transmitted by the *Aedes* mosquitoes. Approximately 100 million individuals are affected by the disease annually and one billion are at risk, mainly in the subtropical regions. Severe forms of the disease can lead to death within hours. There is an urgent need for preventive or curative tools to fight against the dengue virus, because no such specific treatment exists to date. The virus has four serotypes, DEN1 to DEN4. Several tetravalent vaccines are under development but they will not be available for at least a decade, and comprehensive vaccinal coverage might be difficult to achieve [1,2].

The dengue virus is an enveloped RNA virus. The structures of the whole virus and of its envelope glycoprotein E have been elucidated by a combination of

Abbreviations
-, covalent bond; ::, noncovalent bond; CDR, complementary determining region; E3, domain 3 of gpE; gpE, glycoprotein E; H-Trp96, a tryptophan residue in position 96 of the heavy chain; H-W96A, mutation of residue H-Trp96 into Ala; RU, resonance unit; SDR, structure determining residue.

X-ray crystallography and electron cryomicroscopy [3,4]. Ninety dimers of gpE cover the surface of the virus. Each monomer comprises three ectodomains, E1 to E3, and one transmembrane domain, E4. Domain E3, located between E1 and E4, is continuous, comprises residues 296–400 of gpE, and possesses a compact fold which is stabilized by a disulfide bond between residues Cys302 and Cys333. Numerous data indicate that E3 is the primary site of interaction between the virus and receptors at the surface of the target cells [4,5]. Domain E3 is highly immunogenic and many antibodies that are specific for E3 are strong blockers of viral adsorption to cells [6].

Monoclonal antibody mAb4E11 is directed against the DEN1 virus. It recognizes the four serotypes of the dengue virus, but not other flaviruses [7], and neutralizes them with different efficacies [8]. Its epitope is included within domain E3 of gpE [7–9]. It protects against a challenge by the DEN1 virus in a murine experimental model [8]. mAb4E11 therefore constitutes an interesting experimental system to analyze and understand the interactions between antibodies and the dengue virus; in particular, the specificity of recognition towards this virus to the exclusion of other flaviviruses, the cross-reactivities towards the four viral serotypes, and the mechanisms of neutralization at a molecular level.

The diversity of the variable regions of antibodies originates in four different processes: the association of germline genetic segments produces rearranged variable *V* genes, the variability of the junctional sites and the addition or deletion of nucleotides create new codons at the junctions of the genetic segments, the heavy and light chains of immunoglobulins associate randomly and finally the rearranged *V* genes undergo somatic hypermutagenesis [10]. As a result of these four genetic processes, the sequences of antibodies contain six hypervariable regions in the variable (V) domains, three in the heavy chain V_H and three in the light chain V_L, that determine the complementarity with the antigen and are hence named CDRs for complementary determining regions [11]. The structures of the CDR loops are determined by their length and the presence of specific residues. They are distributed into canonical classes. The structure determining residues (SDR) are found both within and outside the CDRs [12–16]. The CDR3 loops of V_H and V_L contain the residues of diversity and junction, encoded by the *D* segment, and the V_H-*D*, *D*-J_H, and V_L-J_L junctions [17]. They are located at the center of the antibody combining site [18,19] and provide the major part of the free energy of interaction with the antigen [20,21].

We have undertaken a detailed analysis of the relations between the structure of antibody mAb4E11 and its properties of interaction with the dengue virus. Here, with the above considerations in mind, we asked the following questions. Can we reconstitute the events of recombination and the somatic hypermutations that resulted in mAb4E11? What are the residues of the CDR3 loops that contribute most strongly to the energy of interaction between mAb4E11 and its antigen, and to their rates of association and dissociation? Is it possible to distinguish between residues that are directly involved in the interaction and those that have a conformational role?

To approach these questions, we exploited the structural and genomic data that are available on antibodies and their genes, and performed a systematic scanning of the CDR3 loops of mAb4E11 by mutagenesis of their residues into alanine (Ala scanning). The affinities of the purified mutant Fab fragments of mAb4E11 for its antigen were measured by a competition ELISA in solution, and their kinetics of interaction with the antigen were measured by surface plasmon resonance. The results showed in particular that the residues of diversity and junction constituted hotspots of binding energy, and were hydrophobic or negatively charged. They will be useful to identify the full epitope of mAb4E11 at the surface of the viral envelope glycoprotein, compare the energetic and kinetic maps of interaction between its paratope and the four viral serotypes, test the relations between affinity and neutralization, and improve its properties for applications in diagnosis and therapy.

Results

Germline gene segments and their rearrangements

We used Chothia's numbering for the amino-acid sequences of immunoglobulins and his definition of the CDR loops (see Experimental procedures) [13]. The limits of the CDRs of antibody mAb4E11 were as follows: Arg24-His34, Arg50-Ser56 and Gln89-Thr97 for V_L; Gly26-Thr32, Asp52-Asp56, and Gly95-Tyr102 for V_H. We identified the germline gene segments of the mouse that have rearranged to form mAb4E11, by using the IMGT data base [22]. The V_L gene derived from the germline segments IGKV3-5*01 and IGKJ1*01, and V_H from the segments IGHV14S1*01, IGHD-Q52*01 and IGHJ3*01. IGHD-Q52*01 is the shortest *D* segment in the mouse. No addition or change of nucleotide was introduced during the formation of the V_κ-J_κ junction. Several deoxyguanosine

V_L

*IGKV3-5*01*

```
 88  89  90  91  92  93  94  95
  C   Q   Q   S   N   E   D   P
-TGT CAG CAA AGT AAT GAG GAT CCT C3'
```

*IGKJ1*01*

```
                                W   T   F
                             5'G TGG ACG TTC-
```

mAb4E11

```
 88  89  90  91  92  93  94  95  96  97  98
  C / Q   R   S   N   E   V   P   W   T / F
-TGT CAG CGA AGT AAT GAG GTT CCT TGG ACA TTC-
```

V_H

*IGHV14S1*01*

```
 92  93  94
  C   A   R
-TGT GCT AGA3'
```

*IGHD-Q52*01*

```
            N   W   D
         5'CT AAC TGG GAC3'
```

*IGHJ3*01*

```
                        W   F   A   Y   W
                     5'CC TGG TTT GCT TAC TGG-
```

mAb4E11

```
 92  93  94  95  96  97  98  99  101 102 103
  C   S   R / G   W   E   G   F   A   Y / W
-TGT TCT AGG GGC TGG GAG GGG TTT GCT TAC TGG-
```

Fig. 1. Genetic rearrangements and hypermutations in the CDR3 loops of mAb4E11. The nucleotide and amino-acid residues that differ between the germline gene segments and mAb4E11 are underlined. The limits of the CDR3 loops are indicated by slashes. The numbering of the residues and the CDR3 loops are defined according to Chothia [13].

residues were introduced during the formation of the V_H-D and D-J_H junctions, likely by the terminal deoxynucleotidyl transferase, and they translate into the amino-acid residues H-Gly95 and H-Gly98, respectively. These residues correspond to the N-regions (Fig. 1).

The identification of the germline gene segments for mAb4E11 enabled us to deduce the somatic hypermutations that are present in its rearranged genes. mAb4E11 contains 12 nonsilent hypermutations, six in V_L and six in V_H. Two mutations are located in L-CDR1 (S28N and S30aR), two in L-CDR3 (Q90R and D94V) and one in H-CDR2 (K56D). The seven other hypermutations are located in framework regions.

Productions of Fab4E11-H6 and its antigen

Fab4E11-H6 is a hybrid between the Fab fragment of antibody mAb4E11 and a hexahistidine tag. The Fab4E11-H6 fragment and its mutant derivatives were produced in the *E. coli* periplasm, an oxidizing cellular environment where the disulfide bonds could form. They were purified from a periplasmic extract by affinity chromatography on a nickel ion column, with a mean yield equal to 500 $\mu g \cdot L^{-1}$ of culture in flask. The purified preparations were homogeneous at more than 90%.

MalE-E3-H6 is a hybrid between the MalE protein from *E. coli,* domain 3 of the envelope glycoprotein E from the dengue virus (serotype DEN1), and a hexahistidine tag, from N- to C-terminus. We produced the MalE-E3-H6 protein in the *E. coli* periplasm for the same reason as above. PD28, the host strain, is deleted for the *malE* gene. We could purify MalE-E3-H6 to full homogeneity by two successive chromatographies, first on an amylose column, then on a nickel ion column, with a yield of 5 $mg \cdot L^{-1}$ of culture in flask. We used MalE-E3-H6 as an antigen for mAb4E11.

We measured the dissociation constant between the Fab4E11-H6 fragment and its MalE-E3-H6 antigen by a competition ELISA in solution, in which the concentration of antigen varied (Fig. 2; Experimental procedures). The low value obtained, $K_D = 0.11 \pm 0.01$ nM,

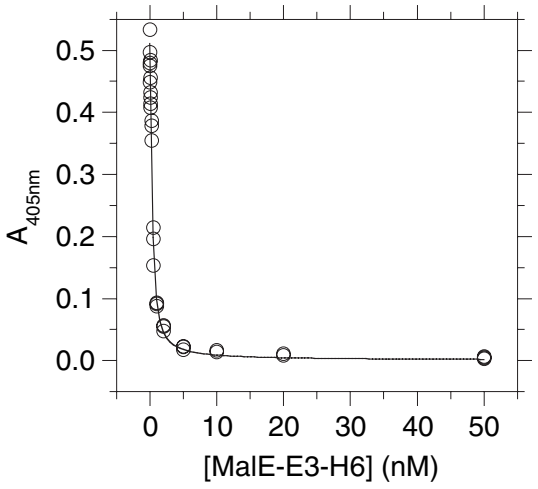

Fig. 2. Determination of the dissociation constant between the Fab4E11-H6 fragment of the wild type and the MalE-E3-H6 antigen by competition ELISA in solution. Fab4E11-H6 and MalE-E3-H6 were first incubated for 20 h at 25 °C in solution until the binding reaction reached equilibrium. The concentration of free Fab4E11-H6 was then measured by an indirect ELISA in which MalE-E3-H6 was immobilized in the wells of a microtiter plate and the bound Fab4E11-H6 was revealed with a goat antibody, directed against mouse Fab and conjugated with alkaline phosphatase. The total concentration of MalE-E3-H6 in the binding reaction is given along the *x* axis, and the optical signal A_{405} in the indirect ELISA is given along the *y* axis. This signal is proportional to the concentration of free Fab4E11-H6 in the binding reaction. The curve was obtained by fitting the equation of the equilibrium to the experimental data as described, with K_D and the maximal value of the signal as fitting parameters [48]. Twelve concentrations were used and each data point was perfomed in triplicate.

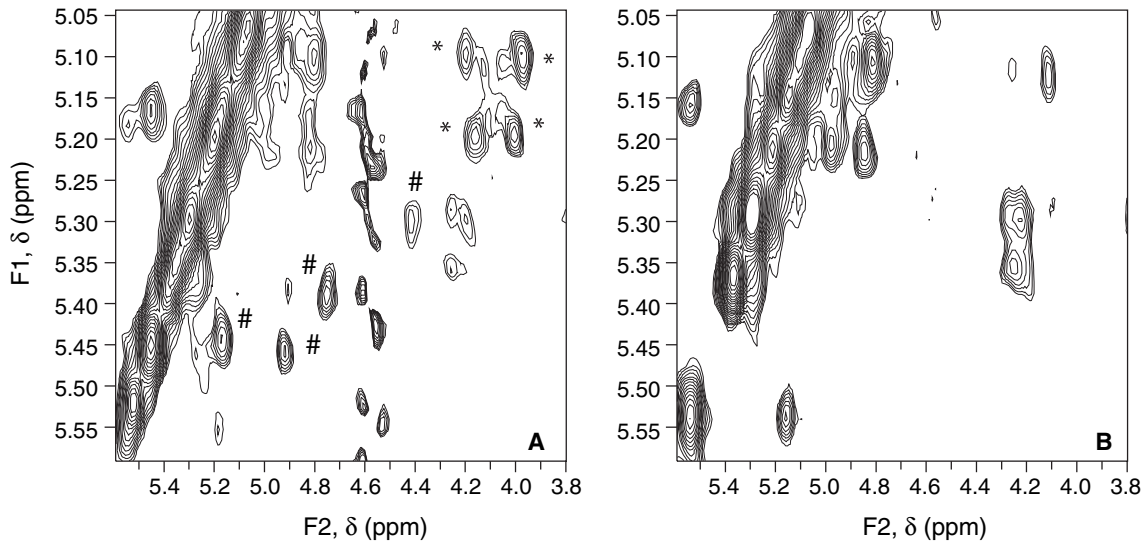

Fig. 3. Comparison of the H_α regions in NOESY spectra of MalE-E3-H6 (A) and MalE (B). The two spectra were acquired at 40 °C in buffer A, prepared in D_2O. They are plotted at the same contour level. δ: chemical shift. #: nOes that were present in the spectrum of MalE-E3-H6 and absent from that of MalE, occurred between protons with high chemical shifts in the F1 dimension, and could be assigned to H_α–H_α interactions. *: intraresidue nOes that were present in the spectrum of MalE-E3-H6 and absent from that of MalE. Peaks at *c.* 4.6 p.p.m. in the F2 dimension correspond to the residual water signal.

suggested that the epitope of mAb4E11 was totally included in domain E3 and that the E3 moiety of the MalE-E3-H6 hybrid was functional for its recognition by the antibody. We have produced domain E3 in an isolated format since the completion of this work and found equal values of K_D for the interactions between Fab4E11-H6 and either Mal-E3-H6 or E3-H6.

Structure of domain E3 within the MalE-E3-H6 hybrid

The structures of glycoproteins E from the DEN2 and DEN3 viruses have been solved (see above). Glycoproteins E from the DEN1 and DEN2 viruses have identical functions and highly similar sequences. The amino-acid sequences of their E3 domains have 65% identity, which strongly suggests that they display the same fold. Domain E3 from the DEN2 virus is an all-β protein that contains three antiparallel β-sheets [3]. Hence, domain E3 from the DEN1 virus should present a high content of antiparallel β-sheets if it were folded within the MalE-E3-H6 hybrid.

^{1}H-NMR experiments were conducted on samples of the MalE-E3-H6 hybrid and wild-type protein MalE to assess whether domain E3 was structured within the hybrid. NMR can readily detect the presence of β-sheets because the chemical shifts have characteristically higher values for H_α protons in β-sheets than for those in unstructured peptides or α-helices [23]. Moreover, the H_α protons in two adjacent antiparallel β-strands can give rise to a dipolar interaction (nOe). A comparison of the NOESY spectra of MalE-E3-H6 and MalE allowed us to unambiguously assign four interstrand H_α-H_α nOe signals to the E3 moiety of the hybrid (Fig. 3). These H_α-H_α nOe signals indicated that at least 12 residues in the E3 moiety of the hybrid belonged to antiparallel β-sheets. Moreover, by comparing NOESY spectra (corresponding to through-space correlations, Fig. 3) and TOCSY spectra (through-bond correlations, not shown) of MalE-E3-H6 and MalE, we identified nine additional H_α protons (two from the NOESY spectrum and seven from the TOCSY spectrum) in the E3 moiety of the hybrid with downfield shifted signals (≥ 5.0 p.p.m). Inspection of NOESY and TOCSY spectra that were acquired under varying experimental conditions, indicated that MalE-E3-H6 did not present large unstructured regions. Altogether, these results indicated that domain E3 was structured and contained a large amount of antiparallel β-sheets within the hybrid used as an antigen. This conclusion is consistent with the reports that domains E3 from several flaviviruses have similar structures in an isolated soluble form and in a crystalline form, integrated within the full length gpE [24,25].

Contribution of the CDR3 loops to the energy of interaction

The CDR3 loops of mAb4E11 comprise nine residues for the V_L domain and seven residues for V_H. Each

residue of the CDR3 loops was changed into Ala by oligonucleotide site-directed mutagenesis, except H-Ala101 which was changed into Gly. The mutant Fab4E11-H6 fragments were purified and their K_D values for the MalE-E3-H6 antigen determined as described for the wild type. The corresponding variations of the free energy of interaction at 25 °C, $\Delta\Delta G$, ranged from 0 to 6 kcal·mol^{-1} (Table 1). The standard error on the values of ΔG were low and allowed us to significantly detect variations $\Delta\Delta G$ as low as 0.3 kcal·mol^{-1}.

The deletion of side-chains by mutation into Ala showed that five residues, L-Ser91, L-Pro95, L-Trp96, H-Trp96 and H-Glu97, were strongly involved in the molecular interaction between Fab4E11-H6 and MalE-E3-H6 ($\Delta\Delta G \geq 2.9$ kcal·mol^{-1}). The effect of mutation H-W96A was so strong that we could not determine it precisely ($\Delta\Delta G > 5.8$ kcal·mol^{-1}). The side chains of L-Gln89, L-Arg90, and L-Asn92 were more weakly involved ($1.1 \leq \Delta\Delta G \leq 1.6$). The side chains of L-Glu93, L-Val94, L-Thr97, H-Phe99, H-Ala101 and H-Tyr102 were apparently not involved.

The mutation of Gly into Ala adds a $C_\beta H_3$ group to the residue and constrains its (φ, ψ) torsion angles [26]. The strong destabilizing effects of mutations H-G95A and H-G98A on the interaction between Fab4E11-H6 and MalE-E3-H6 could therefore be due to steric clashes between the mutant side-chains and either residues of MalE-E3-H6 or neighboring residues of Fab4E11-H6, e.g. H-Trp96 and H-Glu97 which were the most important residues for this interaction (Table 1).

Table 1. Equilibrium constants and associated free energies for the dissociation between MalE-E3-H6 and wild-type or mutant Fab4E11-H6. K_D was measured at 25 °C in solution by a competition ELISA. The mean and associated SE values of K_D, $\Delta G = -RT\ln(K_D)$, and $\Delta\Delta G = \Delta G(\text{WT}) - \Delta G(\text{mut})$ in three independent experiments are given. In addition, each ELISA measurement was performed in triplicate. WT, wild type; mut, mutant. The SE value on $\Delta\Delta G$ was calculated through the formula $[\text{SE}(\Delta\Delta G)]^2 = [\text{SE}(\Delta G(\text{WT}))]^2 + [\text{SE}(\Delta G(\text{mut}))]^2$.

Mutation	K_D (nM)	ΔG (kcal·mol^{-1})	$\Delta\Delta G$ (kcal·mol^{-1})
WT	0.11 ± 0.01	13.61 ± 0.06	0.0 ± 0.1
L-Q89A	1.6 ± 0.2	12.02 ± 0.06	1.6 ± 0.1
L-R90A	0.64 ± 0.04	12.54 ± 0.03	1.1 ± 0.1
L-S91A	13.6 ± 0.6	10.73 ± 0.03	2.9 ± 0.1
L-N92A	0.7 ± 0.1	12.51 ± 0.12	1.1 ± 0.1
L-E93A	0.16 ± 0.05	13.41 ± 0.19	0.2 ± 0.2
L-V94A	0.08 ± 0.02	13.82 ± 0.15	− 0.2 ± 0.2
L-P95A	13 ± 2	10.76 ± 0.07	2.9 ± 0.1
L-W96A	77 ± 26	9.70 ± 0.20	3.9 ± 0.2
L-T97A	0.07 ± 0.01	13.88 ± 0.11	− 0.3 ± 0.1
H-G95A	26 ± 2	10.35 ± 0.05	3.3 ± 0.1
H-W96A	>1500	<7.9	>5.8
H-E97A	1490 ± 800	7.95 ± 0.32	5.7 ± 0.3
H-G98A	22 ± 3	10.45 ± 0.08	3.2 ± 0.1
H-F99A	0.13 ± 0.06	13.58 ± 0.24	0.0 ± 0.3
H-A101G	0.05 ± 0.01	14.03 ± 0.05	− 0.4 ± 0.1
H-Y102A	0.17 ± 0.01	13.32 ± 0.03	0.3 ± 0.1

Kinetics of the interaction

To analyse the contributions of the residues in the CDR3 loops to the kinetics of interaction between the Fab4E11-H6 fragment and its MalE-E3-H6 antigen, we measured the corresponding rate constants, k_{on} and k_{off}, for the wild-type and mutant derivatives of Fab4E11-H6. MalE-E3-H6 was attached to the sensorchip surface and Fab4E11-H6 was in the soluble phase for these experiments, which were performed with the Biacore instrument (Table 2). The association of the wild-type Fab4E11-H6 was fast, with $k_{on} = 3.7 \pm 0.2 \times 10^6$ M^{-1}·s^{-1}, and its dissociation was in the average for Fab fragments, with $k_{off} = 2.6 \pm 0.3 \times 10^{-4}$ s^{-1} [27]. We found that k_{on} varied by less than twofold upon mutation, except in three cases, L-P95A, H-G95A and H-G98A, for which this variation was

Table 2. Kinetic parameters for the interaction between immobilized MalE-E3-H6 and wild type or mutant Fab4E11-H6. The rate constants k_{on} and k_{off} were measured at 25 °C with the Biacore instrument, with MalE–E3-H6 in the immobile phase and Fab4E11-H6 in the mobile phase. The mean and associated SE values of k_{off} in measurements at 8–12 different concentrations of Fab4E11-H6 are given. The SE value on k_{on} was deduced from that on the active concentration C of Fab4E11-H6 through the formula $\text{SE}(k_{on})/k_{on} = \text{SE}(C)/C$. It was not possible to determine k_{on} and k_{off} for the three mutants that were the most affected in the interaction with the antigen. However, it was possible to measure the dissociation constant $K_D' = 518 \pm 31$ nM for the equilibrium between the immobilized antigen and the soluble Fab4E11(H-E97A) mutant.

Mutation	k_{on}(10^6 M^{-1}·s^{-1})	k_{off}(10^{-4} s^{-1})
WT	3.7 ± 0.2	2.6 ± 0.3
L-Q89A	2.7 ± 0.6	31 ± 2
L-R90A	2.6 ± 0.2	8.3 ± 0.8
L-S91A	2.7 ± 0.3	37 ± 5
L-N92A	2.5 ± 0.3	7 ± 1
L-E93A	3.4 ± 0.2	1.4 ± 0.5
L-V94A	2.8 ± 0.3	1.6 ± 0.4
L-P95A	0.58 ± 0.08	4.4 ± 0.7
L-W96A	ND	ND
L-T97A	2.4 ± 0.4	2.2 ± 0.3
H-G95A	0.11 ± 0.02	11 ± 1
H-W96A	ND	ND
H-E97A	ND	ND
H-G98A	0.62 ± 0.09	275 ± 48
H-F99A	3.3 ± 0.1	1.4 ± 0.4
H-A101G	2.9 ± 0.4	1.4 ± 0.7
H-Y102A	6 ± 1	1.5 ± 0.4

equal to 6.3-, 33- and 5.9-fold, respectively. In contrast, k_{off} varied widely, by more than 100-fold. We could not measure k_{on} and k_{off} for the three mutations that affected the interaction with the antigen the most, i.e. L-W96A, H-W96A and H-E97A, because of the low time-resolution of the instrument (2.5 data points per second).

Discussion

Functional importance of the rearrangements and hypermutations

An Ala scanning enabled us to identify the residues of the CDR3 loops that contributed to the energy of interaction between Fab4E11 and its antigen. L-Trp96 was the major contributor of L–CDR3 to this interaction. It corresponds to the junction between the V_κ and J_κ gene segments. H-Gly95, H-Trp96, H-Glu97 and H-Gly98 were the major contributors of H-CDR3. They correspond to the *D* gene segment and to its junctions with the V_H and J_H segments. In particular, H-Gly95 and H-Gly98 correspond to the N-regions. Overall, H-Trp96 was the most important residue of both CDR3 loops. Thus, our results showed that the residues of the CDR3 loops that contributed the most to the energy of interaction, corresponded precisely to those brought by the diversity and junction residues during the rearrangements of the germline gene segments (Table 1 and Fig. 1). The finding that L-Trp96 and H-Trp96 constituted hotspots of binding energy was consistent with the higher abundance of Trp residues in the CDR loops than in the generic protein loops [28].

Mutation L-R90A decreased the energy of interaction between the Fab4E11 fragment and its antigen by 1.1 ± 0.1 kcal·mol^{-1}. This result showed that the side chain of residue L-Arg90 contributed to the interaction with the antigen and was consistent with the selection of hypermutation L-Q90R during the somatic maturation of antibody mAb4E11. Mutation L-V94A had no effect on the energy of interaction, even though residue L-Val94 originates from hypermutation L-D94V (Fig. 1). Neutral hypermutations have previously been observed in the CDR loops of other antibodies [29]. Thus, the two hypermutated residues of the CDR3 loops contributed marginally to the energy of interaction with the antigen when compared to the diversity and junction residues.

Non-additivity of mutations

The variations in the free energy of interaction $\Delta\Delta G$ for the five most destabilizing mutations (excluding H-G95A and H-G98A, see below) had a sum equal to 21.2 kcal·mol^{-1}, i.e. higher than the free energy of interaction $\Delta G = 13.6$ kcal·mol^{-1} between the wild-type Fab4E11 and its antigen. This comparison for Fab4E11 was consistent with the fact that the free energy of interaction between proteins generally results from a small number of strong interactions at the center of the interface, and not from the accumulation of numerous weak contacts [30,31]. It showed that the energetic effects of the individual mutations were not independent, and suggested that some mutations resulted in local conformational changes. The assessment of the direct or indirect effects of mutations on binding is difficult, because it is not feasible to solve the crystal structure of every mutant protein in general. Moreover, small variations in the geometry of the contacts can lead to large variations in the energy of interaction. However, such an assessment is critical if one wants to use mutagenesis data to understand or engineer the energy and specificity of binding rationally [32]. We therefore resorted to the exceptionally large amount of acquired knowledge on antibodies and their interactions.

Direct vs. indirect effects of the mutations

A statistical analysis of 26 complexes between antibodies and antigens whose crystal structures had been solved, has provided the probabilities that the CDR residues form topological contacts with an antigen [19]. We compared these published probabilities and our mutagenesis results to predict which mutations of Fab4E11 might have a direct effect on the interaction, by deletion of noncovalent bonds with the antigen, and which ones might have an indirect conformational effect (columns 2, 3 and 5 of Table 3).

In the V_L domain, the comparison of Table 3 suggested to us that residues L-Ser91, L-Asn92 and L-Trp96 formed direct energetic noncovalent bonds with the antigen, and that the deletion of their side chains beyond the C_β group by mutation into Ala removed or weakened these bonds. They also suggested that the side chains of residues L-Gln89, L-Arg90 and L-Pro95 did not form direct contacts with the antigen and that the effects of their mutations into Ala on the energy of interaction were indirect and conformational.

In V_H, the same comparison suggested that the side chains of residues H-Trp96 and H-Glu97 formed direct noncovalent bonds with the antigen. This analysis was not pertinent for residues H-Gly95 and H-Gly98, which have no side chain and were changed into Ala, a bulkier residue.

Table 3. Direct vs. indirect effects of the mutations in Fab4E11-H6. Columns 2 and 3, frequency of exposed residues in the free antibodies (column 2) and frequency of contact residues in the complexes between antibodies and antigens (column 3) at the residue position of column 1, according to known crystal structures. Data from [19]. Column 4, water accessible surface area for the side chain (sc-ASA) of the wild-type residue in column 1, as measured in a three-dimensional model of Fv4E11 (see Fig. 4). Column 5, variation $\Delta\Delta G$ of the free energy of interaction between Fab4E11-H6 and MalE-E3-H6, resulting from the mutation in column 1 (see Table 1).

Mutation	Exposed (%)	Contact (%)	sc-ASA (Å^2)	$\Delta\Delta G$ (kcal·mol^{-1})
L-Q89A	19	8	0.0	1.6 ± 0.1
L-R90A	8	0	5.7	1.1 ± 0.1
L-S91A	88	81	0.0	2.9 ± 0.1
L-N92A	100	54	19.7	1.1 ± 0.1
L-E93A	100	54	87.8	0.2 ± 0.2
L-V94A	100	81	40.5	− 0.2 ± 0.2
L-P95A	96	0	22.4	2.9 ± 0.1
L-W96A	100	81	18.4	3.9 ± 0.2
L-T97A	100	0	23.9	− 0.3 ± 0.1
H-G95A	81	69	0.0	3.3 ± 0.1
H-W96A	100	58	143	> 5.8
H-E97A	92	85	47.0	5.7 ± 0.3
H-G98A	96	52	0.0	3.2 ± 0.1
H-F99A	86	27	1.9	0.0 ± 0.3
H-A101G	92	4	11.4	− 0.4 ± 0.1
H-Y102A	100	0	58.3	0.3 ± 0.1

Ala mutations and conformational effects

As mentioned above, the mutations of CDR residues into Ala or Gly could affect the interaction between Fab4E11 and its antigen by different mechanisms: the deletion of noncovalent bonds between the mutated residue and the antigen; conformational changes of CDR loops; or a mere destabilization of their active conformation. In an attempt to distinguish between these mechanisms, we predicted the structural classes of the CDRs for the Fab4E11 fragment of the wild type and analyzed the potential effects of some mutations on the corresponding structures. According to the predictions, the structures of L-CDR2 and H-CDR2 were canonical, whereas those of H-CDR1, L-CDR1 and L-CDR3 were similar but not identical to canonical structures. Structural classes exist only for the base of H-CDR3. The H-CDR3 loop of mAb4E11 had a kinked base, and the presence of residue H-Gly98 implied a *gauche* kinked type (K^G). Some mutations that we constructed in Fab4E11, removed a structure determining residue (SDR) for the class of a CDR loop (Table 4).

The predicted structure of the L-CDR3 loop was similar to the canonical structure 1/9A when the residue in position L-90 of Fab4E11 was either Arg as in the wild type or Ala as in the L-R90A mutant. It was identical to 1/9A when residue L-90 was Gln as in the germline antibody (Table 4). The canonical structure 1/9A of L-CDR3 is a β-hairpin, distorted by the *cis*-Pro residue at position L-95 and stabilized by non–covalent interactions between the side-chain of residue L-90, which must be Gln, Asn or His, and other chemical groups of the loop [13,16]. Residue L-Arg90 of Fab4E11 could form some but not all of the stabilizing interactions that are normally made by the germline residue L-Gln90. The mutant residue L-Ala90, which has only a methyl group C_β-H_3 as a side chain, could form none of them. This analysis suggested that mutation L-R90A could destabilize the conformation of L-CDR3 and that its effect on affinity ($\Delta\Delta G$ = 1.1 ± 0.1 kcal·mol^{-1}) could be indirect. The presence of an Arg residue in position L-90 is very rare in antibodies (0.34%, [11]) and, therefore, the potential interdependent effects of hypermutation L-Q90R on affinity and structure deserve a thorougher analysis.

Table 4. Structural classification for the CDR loops of mAb4E11. Columns 2 and 3, structural class of the CDR in column 1, as determined by Martin's program [12] or a manual protocol for H-CDR3 [15]. Column 2 uses Chothia's SDR templates and classes [13,14] whereas column 3 uses Martin's auto-generated SDR templates and classes [12]. = and ≈, identity or mere similarity with the elements of the class, respectively; K^G, *gauche*-kinked type [15]. Column 4, residues of the wild-type mAb4E11 that differ from the SDRs of the class in column 3. L-Asn28 and L-Arg90 correspond to somatic hypermutations, whereas L-Leu2 and H-Lys2 were introduced by the PCR primers during the cloning of the Fab4E11 genes [8]. The structure of L-CDR3 is predicted as canonical if L-Arg90 is reverted into the germline L-Gln90. Column 5, Ala mutations that removed an SDR of the class in column 3.

CDR	Class C	Class M	WT-residues	Ala mutation
L1	≈ 5	≈ 15A	L2, N28, R90	N92A, E93A
L2	= 1	= 7A		
L3	≈ 1	≈ 9A	R90	Q89A, S91A, V94A, P95A, W96A, T97A
H1	= 1	≈ 10A	K2	Y102A
H2	= 2	= 10A		
H3	= K^G	= K^G		G98A

Proline can adopt *cis* and *trans* conformations, contrary to the other residues, which adopt only the *trans* conformation. Proline adopts well-defined (φ, ψ) dihedral angles and constrains the (φ, ψ) angles of the residue on its N-terminal side, which adopts an extended conformation in > 90% of the cases [33]. Therefore, mutation L-P95A of Fab4E11 could modify the structure of L-CDR3 both by changing the conformation of residue L-95 from *cis* to *trans* and relaxing the conformation of the loop. This analysis suggested that

the strong effect of mutation L-P95A on affinity ($\Delta\Delta G = 2.9 \pm 0.1$ kcal·mol^{-1}) resulted from a structural change of L-CDR3 and corresponded to the indirect contribution of an SDR residue, L-Pro95, to affinity through conformation.

Mutations of uncharged residues affect k_{on}

The study of the interactions between proteins by a combined approach of kinetics and mutagenesis, led Schreiber to propose that the transition state for the association is stabilized by specific long–range electrostatic interactions and nonspecific short-range hydrophobic or Van der Waals interactions, and that large portions of the interface are solvated in this state. This mechanism was proposed because only the mutations that involve charged residues, affect k_{on} significantly (more than twofold), whereas the mutations of uncharged residues are neutral towards association although they can strongly affect k_{off} and K_D [34].

Three mutations of Fab4E11, L-P95A, H-G95A and H-G98A, that affected neutral residues of the paratope, strongly decreased k_{on}. They either changed an SDR residue (L-P95A) or added a methyl group to the side chain (H-G95A and H-G98A). Therefore, it is possible that the three mutations had strong effects on k_{on} because they induced conformational changes of the paratope and affected neighboring charged or hydrophobic residues. L-Trp96, H-Trp96 and H-Glu97 constitute obvious candidates for such functionally important adjacent residues.

The values of K_D, measured by competition ELISA, and $K_D' = k_{off}/k_{on}$, measured with the Biacore instrument, cannot generally be compared because K_D is measured in solution whereas K_D' is measured at the interface between a solid and a liquid phase, and calculated as the ratio of two rate constants. However, values of $\Delta\Delta G$ and $\Delta\Delta G'$ for mutant Fab fragments, calculated from values of K_D and K_D', respectively (Table 1), can be compared because the degrees of freedom for the motion of the antigen that are lost upon immobilization, are identical for the wild-type and mutant Fabs [20,35]. We found that the values of $\Delta\Delta G$ and $\Delta\Delta G'$ for the mutant Fab4E11-H6 fragments were related, with a coefficient of linear correlation $R = 0.95$.

Comparison with a structural model of Fv4E11

So far, we discussed our results by comparison with statistical data on antibodies. At this point of our discussion, we constructed a three-dimensional model of Fv4E11, the variable fragment of mAb4E11, with the WAM software (Fig. 4) [16]. From the model, we calculated the (φ, ψ) dihedral angles for the residues in the L-CDR3 loop and compared them with those in the canonical structure L3-κ-1/9A [13]. This comparison showed that the L-CDR3 loop of Fv4E11 had a distorted canonical structure in the model. The (φ, ψ) angles of residues L-Arg90 and L-Val94 to L-Thr97 were within the intervals of allowed values for the canonical structure whereas those for L-Ser91, L-Asn92 and L-Glu93 were outside. The loop was stabilized by several hydrogen bonds in the model, involving the side-chains of L-Arg90, L-Ser91 and L-Thr97. We also observed that the H-CDR3 loop of Fv4E11 had a kinked base in the model. Thus, the structures of L-CDR3 and H-CDR3 in the model were consistent with the predictions of Table 4.

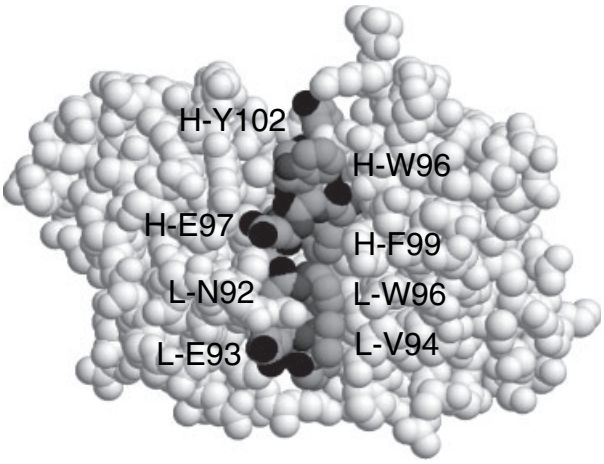

Fig. 4. Positions of the CDR3 loops in a structural model of Fv4E11. The model was generated with the WAM program [16]. The carbon, nitrogen and oxygen atoms are represented in light grey, medium grey and black, respectively. Residues H-Trp96 and H-Glu97 are highly accessible to the solvent, while L-Asn92 and L-Trp96 are partially accessible. They form a continuous patch of accessible surface at the centre of the paratope.

We calculated the water accessible surface area (ASA) of the residues in the three-dimensional model (Table 3). Residues L-Asn92, L-Trp96, H-Glu97 and H-Trp96 formed a continuous patch of exposed residues at the centre of the paratope. H-Glu97 and H-Trp96 were the most exposed residues whereas only the $C_{\zeta 2}$ and $C_{\eta 2}$ groups of L-Trp96 were accessible. Therefore, these four residues could strongly contribute to the free energy of interaction by making direct contacts with the antigen (Table 3). In contrast, L-Gln89 and L-Ser91 were fully buried and L-Arg90 was buried except for its NH_2 group, which was partially accessible. The buried polar or charged groups of these three residues were neutralized by the formation

of hydrogen bonds and the burial of L-Ser91 was clearly linked to the noncanonical structure of the L-CDR3 loop. Residues H-Gly95, H-Gly98 and H-Phe99 were also buried.

Conclusions

We performed a systematic alanine scanning of the L-CDR3 and H-CDR3 loops of antibody mAb4E11. This scanning allowed us to identify the residues of these loops that contributed to the energetics and kinetics of the interaction between mAb4E11 and its antigen. It showed that the residues of diversity, H-Trp96 and H-Glu97, and the residues of junction, L-Trp96, H-Gly95 and H-Gly98, constituted major hotspots of binding energy. It also showed that mutations of neutral residues, L-P95A, H-G95A and H-G98A, decreased the rate of association between Fab4E11 and its antigen.

In the Discussion section, we compared our results first with statistical data on antibodies and then with a three-dimensional model of the Fv4E11 fragment. These comparisons independently suggested that residues L-Trp96, H-Trp96 and H-Glu97 could be in direct contact with the antigen. They showed that mutations L-R90A and L-P95A, which decreased the affinity between Fab4E11 and its antigen, changed residues that generally do not participate in the contacts between antibodies and antigens but determine the structure of L-CDR3. The resolution of the crystal structures of the parental and mutant Fv4E11 fragments, free or in complex with the antigen, could substantiate these points.

Our study raises several fundamental questions on antibodies. Does a tight and general relation exist between the residues of antibodies that provide the diversity of sequence and those that provide the energy of interaction with the antigen? Can a somatic hypermutation, e.g. L-Q90R in mAb4E11, improve the affinity for the antigen by modifying the conformation of a CDR loop? To what extent does the rate of association between antibody and antigen depend on the precise topology of the electrostatic field at the surface of the antibody paratope, in addition to its global charge?

mAb4E11 neutralizes the four serotypes of the dengue virus with varying efficacies [8]. Our results showed that hydrophobic and negatively charged residues of mAb4E11 were major contributors to the binding energy with its antigen. Therefore, they suggested that the epitope of mAb4E11 has both hydrophobic and positively charged components. In fact, this conclusion proved critical to characterize this epitope fully and precisely (O. Lisova, F. Hardy, A. Urvoas, V. Petit and H. Bedouelle, unpublished results). By comparing the effects of the mutations that we constructed in Fab4E11-H6, on its interactions with the different viral serotypes, we hope to understand the structural, kinetic and energetic bases for these cross-reactivities. The characterization of the conformational and functional importance of the residues in the CDR3 loops of mAb4E11 should help us to improve its properties of antigen recognition by a combined approach, based both on the acquired knowledge and *in vitro* directed evolution. Overall, the data reported here constitute an important basis for transforming Fab4E11 into a therapeutic molecule against the dengue virus. A similar study on the epitope of mAb4E11 at the surface of the envelope proteins from the four viral serotypes, will complement the present study and help understand the molecular mechanisms of neutralization by this antibody, with potential vaccinal applications.

Experimental procedures

Media and buffers

The SB medium and phosphate buffer saline ($NaCl/P_i$) have been described [36]. The SB medium was complemented with 1, 5 or 10 $mg{\cdot}mL^{-1}$ glucose to give the SBG1, SBG5 and SBG10 media, respectively. The cultures of recombinant bacteria were performed in the presence of 200 $\mu g{\cdot}mL^{-1}$ ampicillin. The following buffers were used: buffer A, 50 mM Tris/HCl, pH 7.5, 50 mM NaCl; buffer B, 20 mM Tris/HCl, pH 7.9, 500 mM NaCl; buffer C, 20 mM Tris/HCl, pH 7.5, 50 mM NaCl, 2 mM $MgCl_2$; buffer D, 50 mM potassium phosphate, pH 7.0.

Bacterial strains and plasmids

The bacterial strains PD28 [37], HB2151 [38], RZ1032 [39], and plasmids pMad4E11 and pMalE-E3 [8] have been described. pMad4E11 and pMalE-E3 are derivatives of pComb3 [40] and pMal-p (New England Biolabs, Beverly, MA, USA), respectively. Plasmid pPE1 was constructed from pMad4E11. It codes for a hybrid, Fab4E11-H6, between the Fab4E11 fragment (EMBL loci MMU131288 and MMU131289) and a hexahistidine, in the format V_L-C_L::V_H-C_H-His6, where - and :: represent a covalent bond and a non–covalent association, respectively. pPE1 was constructed by excising the gene 3 segment of pMad4E11 with the restriction enzymes *Spe*I and *Eco*RI, and replacing it precisely with six codons of histidine. The expression of Fab4E11-H6 is under control of promoter *plac* in pPE1. Plasmid pLB5 was constructed from pMalE-E3. It codes for a hybrid MalE-E3-H6 between MalE (residues 1–366 of the mature protein), a linker of 15 residues NH2-NSSSVPGRGSIEGRP-COOH, domain E3 (residues

296–400) of gpE from strain FGA/89 of the DEN1 virus [41], and a Leu-Glu-His6 tag, where MalE is the maltose binding protein of *E. coli* [42]. The expression of MalE-E3-H6 is under control of promoter *ptac* and the MalE signal peptide [43] in pLB5.

Construction of mutations in Fab4E11-H6

The mutations were created by site-directed mutagenesis with synthetic oligonucleotides. The mutations of the V_L-C_L gene were introduced into plasmid pPE1 by using a PCR method [44], the SacI restriction site (located at codon positions 1–2 of the mature part of the V_L-C_L gene), and the HpaI site (codons 128–130). The mutations of the V_H-C_H gene were created by using the single-stranded DNA of pPE1 as a template for mutagenesis [39]. The sequences of the mutant genes were verified.

Production and purification of proteins

The MalE-E3-H6 hybrid protein was produced in the PD28(pLB5) recombinant strain. Bacteria were grown overnight at 30 °C in SBG5 medium, harvested by centrifugation, and resuspended in fresh SBG5 medium to obtain an initial absorbance $A_{600} = 1.25$. They were grown at 22 °C until $A_{600} = 2.5$ and then induced during 2 h with 0.2 mM IPTG for the expression of the recombinant gene. The following steps were performed at 4 °C in buffer A. The bacteria were harvested by centrifugation, resuspended in 1 mg·mL^{-1} Polymyxin B sulfate (Sigma-Aldrich, St Louis, MO, USA; 25 mL for 1 L of initial culture) with stirring for 30 min, then centrifuged at 15 000 ***g*** for 30 min. The supernatant (periplasmic fluid) was loaded onto a column of amylose resin (New England Biolabs; 2 mL of resin for 1 L of initial culture) and MalE-E3-H6 was purified by affinity chromatography as described [45].

The Fab4E11-H6 fragment and its mutant derivatives were produced in the HB2151(pPE1) recombinant strain and its mutant derivatives. The bacteria were grown overnight at 30 °C in SBG10 medium, harvested by centrifugation, and resuspended in SBG1 medium to obtain an initial absorbance $A_{600} = 0.25$. They were grown at 22 °C until $A_{600} = 0.5$ and then induced for 2 h with 0.2 mM IPTG to obtain the expression of the recombinant genes. The concentrations of glucose in the media were chosen to favor the catabolite repression of promoter *plac* during the preculture and minimize it during the expression culture. The following steps were performed at 4 °C in buffer B. The bacteria were harvested, resuspended in 1 mg·mL^{-1} Polymyxin B sulfate, 5 mM imidazole, and their periplasmic fluid was prepared as above.

The preparation of MalE-E3-H6, partially purified by affinity chromatography on amylose resin (see above), and the periplasmic preparations of the Fab4E11-H6 derivatives were purified by affinity chromatography on an Ni-NTA column (Qiagen, Hilden, Germany; 1 mL of resin per 1 L of initial culture). The molecules that bound to the column, were washed with 40 mM imidazole (20 volumes of resin), then eluted with 100 mM imidazole in buffer B. The purity of the preparations was checked by SDS/PAGE. The concentration of the purified MalE-E3-H6 hybrid was determined by using A_{280} and its ε_{280} value, calculated from its amino-acid sequence as described (76445 M^{-1}·cm^{-1}) [46]. The concentrations of the purified Fab4E11-H6 fragments were measured with the Biorad Protein Assay Kit (Biorad, Hercules, CA, USA) and BSA as a standard.

Determination of the equilibrium constants by ELISA

The dissociation constants at equilibrium in solution, K_D, between the Fab4E11-H6 fragment or its mutant derivatives and the MalE-E3-H6 antigen were measured by a competition ELISA [47] with a modification in the mathematical processing of the raw data, as previously described [48]. The measurements were performed at 25 °C in NaCl/P_i containing 1% BSA. Fab4E11-H6 at a constant concentration and MalE-E3-H6 at 12 different concentrations were first incubated together in solution for 20 h, to reach equilibrium. The concentration of free Fab4E11-H6 was then measured by an indirect ELISA, in a microtiter plate whose wells had been coated with a 0.5 μg·mL^{-1} solution of MalE-E3-H6. The bound molecules of Fab4E11-H6 were revealed with a goat anti-(mouse IgG) Ig, Fab specific and conjugated with alkaline phosphatase (Sigma).

Determination of the rate and equilibrium constants with the Biacore instrument

We used mAb56.5, directed against protein MalE, to capture the MalE-E3-H6 antigen in a homogeneous orientation [20,49]. mAb56.5 was covalently immobilized on the carboxymethylated dextran surface of a CM5 sensorchip to a level of 7000–8000 resonance units (RU), using the Amine Coupling Kit (Biacore, Uppsala, Sweden). The resulting derivatized surface, CM5–mAb56.5, was equilibrated with 0.005% detergent P20 (Amersham Biosciences, Uppsala, Sweden) in NaCl/P_i at a temperature of 25 °C and a flow rate of 20 μL·min^{-1}, conditions which were used in all the subsequent steps. In a first experiment, a solution of MalE-E3-H6 alone was injected onto the CM5-mAb56.5 surface, yielding the sensorgram R(MalE-E3-H6). In a second experiment, 150 RU of MalE-E3-H6 were captured on the CM5-mAb56.5 surface as above, and then 10–12 different concentrations of wild-type or mutant Fab4E11-H6 fragment were injected onto the complex CM5-mAb56.5:: MalE-E3-H6. In a control experiment, the background signal was determined by injecting the Fab4E11-H6 derivative alone across the CM5-mAb56.5 surface, without prior

capture of MalE-E3-H6. R(Fab4E11-H6), the sensorgram due to the specific binding of Fab4E11-H6 to MalE-E3-H6, was obtained by subtracting R(MalE-E3-H6) (first experiment) and the background signal (control experiment) from the sensorgram measured in the second experiment. At the end of each experiment, the CM5-mAb56.5 surface was regenerated by injecting 5 μL of 50 mM HCl. The kinetic data were analysed with the BIAEVALUATION 3.0 software (Biacore). The active concentration of each Fab4E11-H6 preparation was determined as described [50]. Briefly, 500 RU of MalE-E3-H6 was captured on the CM5–mAb56.5 surface, and a sample of the Fab4E11-H6 derivative was injected onto the complex at seven different flow rates (2, 5, 10, 20, 30, 50 and 100 $\mu L \cdot min^{-1}$). The resulting sensorgrams were analysed using the BIA-CONC program [51].

NMR

The MalE-E3-H6 sample was prepared by dialysis of the purified protein against buffer D and concentrated using Centricon tubes (Amicon, Beverly, MA, USA). The buffer was exchanged against buffer D prepared in D_2O during the concentration step. Protein MalE was purified as described [52] and kept in ammonium sulfate. It was resuspended in buffer D, extensively dialyzed against 50 mM ammonium bicarbonate, lyophilized and then dissolved in buffer D prepared in D_2O. Maltose in deuterated buffer D was added to each protein sample to ensure that the MalE binding site was occupied. The final protein concentration was 0.25 mM. The NMR experiments were performed at 40 °C and a ^1H resonance frequency of 500 MHz on a Varian Inova spectrometer. Spectra were analyzed with the software VNMR 6.1C (Varian, Palo-Alto, CA, USA). NOESY and TOCSY spectra were recorded with mixing times of 80 ms and 40 ms, respectively [53,54].

Analysis and modeling of sequences and structures

We used Chothia's scheme for the numbering of the amino-acid sequences of immunoglobulins and the definition of their CDR loops, as described from 1997 [13]. The numbering and definition of the L-CDR3 and H-CDR3 loops of mAb4E11 are identical with the Chothia's and Kabat's schemes (http://www.bioinf.org.uk). The three dimensional model of the Fv4E11 fragment was constructed with the WAM program as described [16,55]. The model was verified with the PROCHECK program and analyzed with the WHAT IF program as described [55,56].

Acknowledgements

We thank M. Bumke, N. Failloux and R. Nageotte for genetic constructions, J. M. Betton for purified protein MalE, V. Deubel and P. Lafaye for helpful discussions, and Shamila Naïr for critical reading of the manuscript. This research was funded by grants from the French Ministry of Defense (DGA contract N°01 34 062) and the European Commission (INCO-DEV, contract DENFRAME N°517711) to H. B., and a Marie Curie intra-European-fellowship to O. L. (contract N° MEIF-CT-2003–501066).

References

1 Halstead SB & Deen J (2002) The future of dengue vaccines. *Lancet* **360**, 1243–1245.
2 Gubler DJ (2002) Epidemic dengue/dengue hemorrhagic fever as a public health, social and economic problem in the 21st century. *Trends Microbiol* **10**, 100–103.
3 Modis Y, Ogata S, Clements D & Harrison SC (2003) A ligand-binding pocket in the dengue virus envelope glycoprotein. *Proc Natl Acad Sci USA* **100**, 6986–6991.
4 Mukhopadhyay S, Kuhn RJ & Rossmann MG (2005) A structural perspective of the flavivirus life cycle. *Nat Rev Microbiol* **3**, 13–22.
5 Hurrelbrink RJ & McMinn PC (2003) Molecular determinants of virulence: the structural and functional basis for flavivirus attenuation. *Adv Virus Res* **60**, 1–42.
6 Crill WD & Roehrig JT (2001) Monoclonal antibodies that bind to domain III of dengue virus E glycoprotein are the most efficient blockers of virus adsorption to Vero cells. *J Virol* **75**, 7769–7773.
7 Megret F, Hugnot JP, Falconar A, Gentry MK, Morens DM, Murray JM, Schlesinger JJ, Wright PJ, Young P, Van Regenmortel MH & Deubel V (1992) Use of recombinant fusion proteins and monoclonal antibodies to define linear and discontinuous antigenic sites on the dengue virus envelope glycoprotein. *Virology* **187**, 480–491.
8 Thullier P, Lafaye P, Megret F, Deubel V, Jouan A and Mazie JC (1999) A recombinant Fab neutralizes dengue virus *in vitro*. *J Biotechnol* **69**, 183–190.
9 Thullier P, Demangel C, Bedouelle H, Megret F, Jouan A, Deubel V, Mazie JC & Lafaye P (2001) Mapping of a dengue virus neutralizing epitope critical for the infectivity of all serotypes: insight into the neutralization mechanism. *J General Virol* **82**, 1885–1892.
10 Max EE (2003) Immunoglobulins: molecular genetics. In *Fundamental Immunology*, 5th edn. (Paul WE, ed.), pp. 107–158. Lippincott. Williams and Wilkins, Philadelphia, PA, USA.
11 Johnson G & Wu TT (2000) Kabat database and its applications: 30 years after the first variability plot. *Nucleic Acids Res* **28**, 214–218.
12 Martin AC & Thornton JM (1996) Structural families in loops of homologous proteins: automatic classification, modelling and application to antibodies. *J Mol Biol* **263**, 800–815.

13 Al-Lazikani B, Lesk AM & Chothia C (1997) Standard conformations for the canonical structures of immunoglobulins. *J Mol Biol* **273**, 927–948.
14 Morea V, Tramontano A, Rustici M, Chothia C & Lesk AM (1998) Conformations of the third hypervariable region in the VH domain of immunoglobulins. *J Mol Biol* **275**, 269–294.
15 Shirai H, Kidera A & Nakamura H (1999) H3-rules: identification of CDR-H3 structures in antibodies. *FEBS Lett* **455**, 188–197.
16 Whitelegg N & Rees AR (2004) Antibody variable regions: toward a unified modeling method. *Methods Mol Biol* **248**, 51–91.
17 Tonegawa S (1983) Somatic generation of antibody diversity. *Nature* **302**, 575–581.
18 Tomlinson IM, Walter G, Jones PT, Dear PH, Sonnhammer EL & Winter G (1996) The imprint of somatic hypermutation on the repertoire of human germline V genes. *J Mol Biol* **256**, 813–817.
19 MacCallum RM, Martin AC & Thornton JM (1996) Antibody–antigen interactions: contact analysis and binding site topography. *J Mol Biol* **262**, 732–745.
20 England P, Bregegere F & Bedouelle H (1997) Energetic and kinetic contributions of contact residues of antibody D1.3 in the interaction with lysozyme. *Biochemistry* **36**, 164–172.
21 Xu JL & Davis MM (2000) Diversity in the CDR3 region of V_H is sufficient for most antibody specificities. *Immunity* **13**, 37–45.
22 Lefranc MP (2003) IMGT, the international ImMunoGeneTics database. *Nucleic Acids Res* **31**, 307–310.
23 Wishart DS, Sykes BD & Richards FM (1992) The chemical shift index: a fast and simple method for the assignment of protein secondary structure through NMR spectroscopy. *Biochemistry* **31**, 1647–1651.
24 Wu KP, Wu CW, Tsao YP, Kuo TW, Lou YC, Lin CW, Wu SC & Cheng JW (2003) Structural basis of a flavivirus recognized by its neutralizing antibody: solution structure of the domain III of the Japanese encephalitis virus envelope protein. *J Biol Chem* **278**, 46007–46013.
25 Volk DE, Beasley DWC, Kallick DA, Holbrook MR, Barrett ADT & Gorenstein DG (2004) Solution structure and antibody binding studies of the envelope protein domain III from the New York strain of West Nile Virus. *J Biol Chem* **279**, 38755–38761.
26 Ramachandran GN & Sasisekharan V (1968) Conformation of polypeptides and proteins. *Adv Protein Chem* **23**, 283–438.
27 Foote J & Eisen HN (1995) Kinetic and affinity limits on antibodies produced during immune responses. *Proc Natl Acad Sci USA* **92**, 1254–1256.
28 Collis AV, Brouwer AP & Martin AC (2003) Analysis of the antigen combining site: correlations between length and sequence composition of the hypervariable loops and the nature of the antigen. *J Mol Biol* **325**, 337–354.
29 England P, Nageotte R, Renard M, Page AL & Bedouelle H (1999) Functional characterization of the somatic hypermutation process leading to antibody D1.3, a high affinity antibody directed against lysozyme. *J Immunol* **162**, 2129–2136.
30 Clackson T & Wells JA (1995) A hot spot of binding energy in a hormone–receptor interface. *Science* **267**, 383–386.
31 Bogan AA & Thorn KS (1998) Anatomy of hot spots in protein interfaces. *J Mol Biol* **280**, 1–9.
32 DeLano WL (2002) Unraveling hot spots in binding interfaces: progress and challenges. *Curr Opin Struct Biol* **12**, 14–20.
33 MacArthur MW & Thornton JM (1991) Influence of proline residues on protein conformation. *J Mol Biol* **218**, 397–412.
34 Schreiber G (2002) Kinetic studies of protein–protein interactions. *Curr Opin Struct Biol* **12**, 41–47.
35 Cunningham BC & Wells JA (1993) Comparison of a structural and a functional epitope. *J Mol Biol* **234**, 554–563.
36 Sambrook J, Fritsch EF & Maniatis T (1989) *Molecular Cloning: a Laboratory Manual*, 2nd edn. Cold Spring. Harbor Laboratory Press, Cold Spring Harbor, NY, USA.
37 Duplay P, Szmelcman S, Bedouelle H & Hofnung M (1987) Silent and functional changes in the periplasmic maltose-binding protein of *Escherichia coli* K12: I. transport of maltose. *J Mol Biol* **194**, 663–673.
38 Carter P, Bedouelle H & Winter G (1985) Improved oligonucleotide site-directed mutagenesis using M13 vectors. *Nucleic Acids Res* **13**, 4431–4443.
39 Kunkel TA, Roberts JD & Zakour RA (1987) Rapid and efficient site-specific mutagenesis without phenotypic selection. *Methods Enzymol* **154**, 367–382.
40 Barbas CF III, Kang AS, Lerner RA & Benkovic SJ (1991) Assembly of combinatorial antibody libraries on phage surfaces: the gene III site. *Proc Natl Acad Sci USA* **88**, 7978–7982.
41 Despres P, Frenkiel MP & Deubel V (1993) Differences between cell membrane fusion activities of two dengue type-1 isolates reflect modifications of viral structure. *Virology* **196**, 209–219.
42 Duplay P, Bedouelle H, Fowler AV, Zabin I, Saurin W & Hofnung M (1984) Sequences of the malE gene and of its product, the maltose binding protein of *Escherichia coli* K12. *J Biol Chem* **259**, 10606–10613.
43 Bedouelle H, Bassford PJ Jr, Fowler AV, Zabin I, Beckwith J & Hofnung M (1980) Mutations which alter the function of the signal sequence of the maltose binding protein of *Escherichia coli*. *Nature* **285**, 78–81.
44 Ito W, Ishiguro H & Kurosawa Y (1991) A general method for introducing a series of mutations into

cloned DNA using the polymerase chain reaction. *Gene* **102**, 67–70.
45 Bedouelle H & Duplay P (1988) Production in *E.coli* and one-step purification of bifunctional hybrid proteins which bind maltose. Export of the Klenow polymerase into the periplasmic space. *Eur J Biochem* **171**, 541–549.
46 Pace CN, Vajdos F, Fee L, Grimsley G & Gray T (1995) How to measure and predict the molar absorption coefficient of a protein. *Protein Sci* **4**, 2411–2423.
47 Friguet B, Chaffotte AF, Djavadi-Ohaniance L & Goldberg ME (1985) Measurements of the true affinity constant in solution of antigen-antibody complexes by enzyme-linked immunosorbent assay. *J Immunol Meth* **77**, 305–319.
48 Rondard P, Goldberg ME & Bedouelle H (1997) Mutational analysis of an antigenic peptide shows recognition in a loop conformation. *Biochemistry* **36**, 8962–8968.
49 Guermonprez P, England P, Bedouelle H & Leclerc C (1998) The rate of dissociation between antibody and antigen determines the efficiency of antibody-mediated antigen presentation to T cells. *J Immunol* **161**, 4542–4548.
50 Zeder-Lutz G, Benito A & Van Regenmortel MH (1999) Active concentration measurements of recombinant biomolecules using biosensor technology. *J Mol Recognit* **12**, 300–309.
51 Christensen LL (1997) Theoretical analysis of protein concentration determination using biosensor technology under conditions of partial mass transport limitation. *Anal Biochem* **249**, 153–164.
52 Betton JM & Hofnung M (1996) Folding of a mutant maltose-binding protein of *Escherichia coli* which forms inclusion bodies. *J Biol Chem* **271**, 8046–8052.
53 States DJ, Haberkorn RA & Ruben DJ (1982) A two dimensional nuclear Overhauser experiment with pure absorption phase in four quadrants. *J Magn Reson* **48**, 286–292.
54 Griesinger C, Otting G, Wüthrich K & Ernst RR (1988) Clean Tocsy for ^{1}H spin system identification in macromolecules. *J Am Chem Soc* **110**, 7870–7872.
55 Renard M, Belkadi L & Bedouelle H (2003) Deriving topological constraints from functional data for the design of reagentless fluorescent immunosensors. *J Mol Biol* **326**, 167–175.
56 Renard M, Belkadi L, Hugo N, England P, Altschuh D & Bedouelle H (2002) Knowledge-based design of reagentless fluorescent biosensors from recombinant antibodies. *J Mol Biol* **318**, 429–442.